

# Secondary Cooling in the Direct-Chill Casting of Magnesium Alloy AZ31

E. CARON and M.A. WELLS

Secondary cooling information is critical when modeling the direct-chill (DC) casting process of magnesium alloys. However, accurate data for the heat flux in the secondary cooling zone are scarce, and most reported research is concerned with the DC casting of aluminum alloys. Cooling experiments that simulated the secondary cooling of magnesium AZ31 were conducted in order to observe the influence of various parameters on the different boiling-water heat-transfer phenomena. The heat flux in each boiling regime was quantified as a function of the cooling-water flow rate, water temperature, and initial sample temperature. Equations developed from the cooling experiments could be combined to build “idealized” boiling curves for a given set of DC casting conditions.

DOI: 10.1007/s11663-009-9254-y

© The Minerals, Metals & Materials Society and ASM International 2009

## I. INTRODUCTION

FROM a historical perspective, the direct-chill (DC) casting of magnesium was first used extensively during World War II. Magnesium extrusion billets and rolling ingots were produced for the manufacture of aircraft as well as other military applications. Nowadays, approximately 20 pct of the total magnesium production is done *via* the DC casting process.<sup>[1]</sup> Eighty percent of DC-cast products consist of pure magnesium for alloying purposes (*e.g.*, in aluminum alloys or nodular cast iron), whereas the remaining 20 pct are magnesium wrought alloys such as AZ91, AM60, or AZ31. However, the tolerance for process scrap that prevailed during World War II is no longer economically viable. In order to grow, the magnesium industry will have to improve its understanding of the DC casting process and overcome a number of significant obstacles.

One of the problems that plague the DC casting process is the formation of defects such as center cracks and surface folds. Magnesium alloys with a wide freezing range (*e.g.*, AZ91) are particularly sensitive to crack formation. In comparison to the DC casting of aluminum alloys, the DC casting of magnesium presents the additional problem that these defects are compounded in subsequent rolling operations due to the hcp structure of magnesium.<sup>[1]</sup> Another particularity of magnesium DC casting is the relatively low volumetric heat capacity, which allows the molten metal to freeze more rapidly and renders the process startup even more critical. Finally, in addition to the risk of water entrapment and steam explosions present in the DC

casting of aluminum, the DC casting of magnesium can also lead to a hydrogen explosion if liquid metal from a bleedout comes into contact with water.

Mathematical models of the DC casting process can improve the design and control of this process, and thus help prevent the formation of defects. Thermal models, which predict the temperature profile within the cast product, require accurate boundary conditions at the surface, where primary and secondary cooling takes place. The different boiling-water heat-transfer phenomena that take place during secondary cooling are associated with a wide range of heat fluxes; boiling curves, which express the relationship between the surface heat flux and the surface temperature, are known to be strongly nonlinear. Precise knowledge of the heat flux in each boiling-water regime, and of the parameters that influence it, is therefore required in order to model the DC casting process and reduce the incidence of defect formation.

The research described in this article was an investigation of the effect of various parameters on the boiling-water heat-transfer phenomena during the secondary cooling of magnesium AZ31. This article first introduces the DC casting process, and presents the four different boiling regimes that can take place in the secondary cooling zone. It then summarizes the research already conducted by other authors on the DC casting of magnesium and aluminum alloys. The experimental water-jet rig used to simulate the secondary cooling of magnesium AZ31 and the inverse heat-conduction (IHC) algorithm employed to calculate the surface heat flux and temperature are then described. The heat flux in each boiling regime is quantified as a function of various parameters: the cooling-water flow rate, initial sample temperature, and water temperature. Finally, the different empirical equations developed in this research are combined to build idealized boiling curves and are compared to boiling curves previously used to model the DC casting of magnesium AZ31 but developed based on the secondary cooling of aluminum alloys.

E. CARON, Postdoctoral Fellow, is with the Department of Materials Engineering, University of British Columbia, Vancouver, BC, Canada V6T 1Z4. Contact e-mail: Etienne.Caron@ubc.ca M.A. WELLS, Associate Professor, is with the Department of Mechanical and Mechatronics Engineering, University of Waterloo, Waterloo, ON, Canada N2L 3G1.

Manuscript submitted November 5, 2008.

Article published online June 23, 2009.

## II. BACKGROUND

Figure 1 shows a schematic representation of the DC casting process. This process relies on a water-cooled copper or aluminum mold that is filled with molten metal through a feeder. The removal of heat through the mold wall is referred to as primary cooling. The cooling water exits the mold bottom through an array of holes to produce a series of water jets. This direct contact between cooling water and the ingot or billet surface constitutes secondary cooling. Secondary cooling is responsible for the largest amount (*circa* 80 pct) of heat extraction during steady-state operation<sup>[4]</sup> and is associated with the formation of significant thermal gradients.

As shown in Figure 2, the secondary cooling zone can be divided into an impingement zone (IZ), in which the water jets hit the ingot or billet surface, and a free-falling zone (FFZ), in which the water film flows down the surface.<sup>[5]</sup> The IZ is characterized by a drop in water pressure (corresponding to the variation in momentum) as the water-falling velocity increases. On the other hand, the water pressure in the FFZ is constant and the water velocity in this region depends only on gravitational acceleration.

Mathematical models for the DC casting process have been known to rely on various assumptions to quantify the heat transfer in the secondary cooling zone. Early models<sup>[6-8]</sup> were based on external boundary conditions of the Dirichlet type, *i.e.*, a fixed surface temperature:

$$T_s|_{x=x_{\max}} = T_f \quad [1]$$

in which  $T_f$  corresponded to the cooling-water temperature. Later models<sup>[9,10]</sup> specified a constant heat-transfer coefficient,  $h$ , in the secondary cooling zone:

$$-k \frac{\partial T_s}{\partial x} \Big|_{x=x_{\max}} = h(T_s - T_f) \quad [2]$$

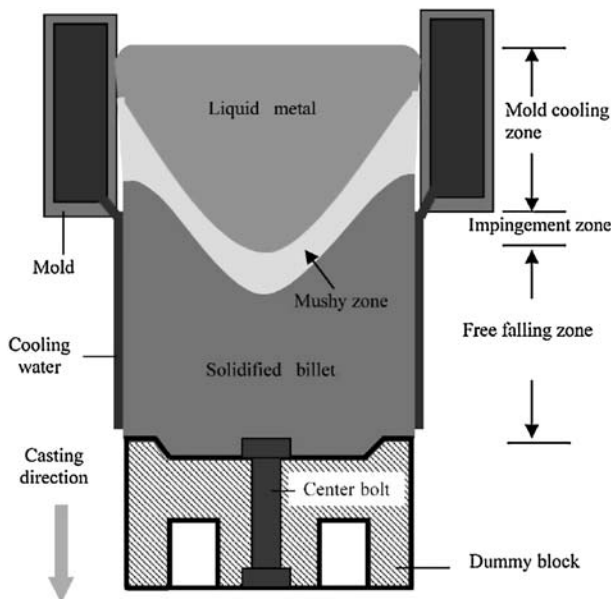


Fig. 1—Schematic of the vertical DC casting process for magnesium billets.<sup>[2]</sup>

or combined boundary conditions of the Dirichlet and Cauchy types.<sup>[11,12]</sup> Recent mathematical models<sup>[5,13,14]</sup> evaluate the surface heat flux using idealized, nonlinear boiling curves:

$$-k \frac{\partial T_s}{\partial x} \Big|_{x=x_{\max}} = \Phi \quad [3]$$

where the heat flux,  $\Phi$ , is a function of the surface temperature,  $T_s$ .

Figure 3 illustrates a typical steady-state boiling curve and shows the four boiling-water heat-transfer regimes that can take place in the secondary cooling zone of the DC casting process: forced convection (FC), nucleate boiling (NB), transition boiling (TB) and film boiling (FB).<sup>[15]</sup> The FB takes place at high surface temperatures  $T_s$ , when a stable vapor layer covers the surface and reduces the heat transfer. Below the Leidenfrost point,  $T_{LPT}$ , this vapor layer breaks down and allows partial wetting of the ingot surface. This corresponds to the TB regime. The critical heat flux (CHF) is the upper limit of the boiling curve and the boundary between TB

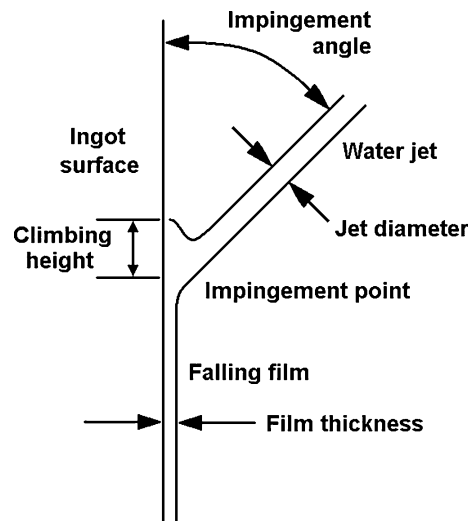


Fig. 2—Geometry of cooling-water jet.<sup>[3]</sup>

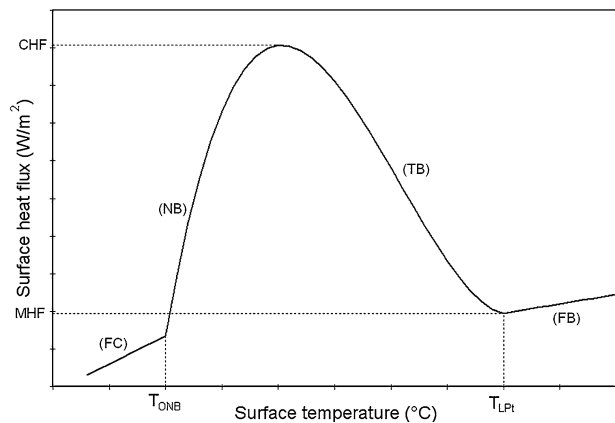


Fig. 3—Schematic of a typical boiling curve.

and NB, in which vapor bubbles are formed at the surface. Finally, below the onset of NB,  $T_{\text{ONB}}$ , heat is removed solely through FC.

Boiling curves for the DC casting of magnesium could not be found in the published literature. A quantification of the heat transfer in the secondary cooling zone during steady state was conducted by Hibbins.<sup>[16]</sup> Thermocouples cast into an AZ31 ingot allowed a calculation of the heat-transfer coefficient  $h$ . Heat-transfer coefficients between 1700 and 7000 W/m<sup>2</sup>·K were identified at the water-jet-impingement point, whereas the water-film FFZ was characterized by heat-transfer coefficients between 10,000 and 12,000 W/m<sup>2</sup>·K. The surface heat transfer was also found to be related to the casting speed and the cooling-water flow rate.

This lack of data for the secondary cooling of magnesium has forced researchers to rely either on simple boundary conditions of the Cauchy type or on boiling curves for the secondary cooling of aluminum alloys. Thus, Le *et al.*<sup>[17]</sup> assumed that only FC with a given heat-transfer coefficient,  $h_{\text{FC}}$ , took place. Meanwhile, Hao *et al.*<sup>[2]</sup> designed a model in which boiling curves for the DC casting of aluminum were modified to fit with measurements from plant trials.

Although the effect of specific properties of magnesium (*e.g.*, surface roughness, thermal conductivity, and specific heat) on the boiling curve is not known with sufficient precision to allow an extrapolation of the results obtained for the DC casting of aluminum, a review of the latter research provides qualitative information regarding the influence of various parameters. For example, quenching tests conducted by Yu<sup>[18]</sup> showed the influence of cooling-water quality on the boiling curve. Surface-tension-lowering surfactants, coagulants, and suspended solids were all found to lower the Leidenfrost point. Similar experiments conducted by Langlais *et al.*<sup>[19]</sup> showed that mold lubricant contamination in the cooling water generally decreases the surface heat flux, because it prevents the formation of steam bubbles.

Other authors used cast-in thermocouples to evaluate the surface heat flux during the casting process. Early experiments by Jensen *et al.*,<sup>[20]</sup> Bakken and Bergström,<sup>[21]</sup> and Tarapore<sup>[22]</sup> were conducted during the steady-state phase of the process. A temperature drop was observed to take place before the water-jet impingement. This phenomenon, which is caused by axial heat conduction in light metals with a high thermal conductivity, is referred to as the advanced cooling front (ACF). Calculations that assume a purely unidimensional heat flow toward the quenched surface, *i.e.*, that do not take into account the effect of the ACF, end up overestimating the surface heat flux in the region above the IZ.

Wiskel and Cockcroft<sup>[23,24]</sup> used a two-dimensional IHC analysis to calculate the surface heat flux during plant trials. Differences were observed between the secondary cooling during the transient start-up phase and in steady state. A similar analysis of plant trials conducted by Kuwana *et al.*<sup>[25]</sup> showed how the cooling-water flow rate increases the heat flux for all boiling regimes in steady state.

The secondary cooling in the DC casting of aluminum alloys was also extensively investigated using samples instrumented with thermocouples and quenched with water jets. While conducting such experiments, Kraushaar *et al.*<sup>[26]</sup> found that the surface heat flux generally increased with an increase in the initial sample temperature  $T_0$ . Maenner *et al.*<sup>[27]</sup> compiled boiling curves calculated by various authors. The different boiling curves showed a very good agreement in the lower-temperature boiling regimes (*i.e.*, FC, NB) but a significant amount of scatter at high surface temperatures.

In order to simulate the steady-state phase of the DC casting process, Grandfield *et al.*<sup>[3]</sup> added a heat source at the back of the instrumented sample so as to compensate for the heat losses at the quenched surface. In steady-state, the cooling-water flow rate  $Q$  was found to increase the heat transfer by FC,  $\Phi_{\text{FC}}$ , as well as the Leidenfrost point,  $T_{\text{LPt}}$ , but did not influence the heat flux in the NB regime,  $\Phi_{\text{NB}}$ .

Larouche *et al.*<sup>[28]</sup> used silver samples instrumented with subsurface thermocouples to investigate the secondary cooling zone of the DC casting process at elevated temperatures. Quenching experiments conducted with pulsed water confirmed the effect of the initial sample temperature already reported by Kraushaar *et al.*:<sup>[26]</sup> each water pulse was characterized by a different start temperature,  $T_0$ , and a distinct boiling curve. Larouche *et al.* also found a linear relationship between the heat flux in the FB regime,  $\Phi_{\text{FB}}$ , and the water flow rate  $Q$ .

Instead of quenching stationary samples with jets of cooling water, Opstelten and Rabenberg<sup>[29]</sup> simulated the secondary cooling with jets in motion with respect to the instrumented sample. Boiling curves obtained with moving water jets were found to differ significantly from the boiling curves for a stationary sample. Opstelten and Rabenberg also identified a relationship between the thermal conductivity of the sample material,  $k_s$ , and the heat flux in the NB and TB regimes.

Kiss *et al.*<sup>[30]</sup> conducted quenching tests on samples with a typical DC-cast surface as well as on samples with a smooth, machined surface. Surface irregularities were shown to promote the formation and anchoring of large bubble patches that generally decrease the heat flux. Similar results were also observed by Li *et al.*<sup>[31]</sup>

Quenching tests conducted by Yu<sup>[32]</sup> allowed the development of equations to relate the Leidenfrost point temperature,  $T_{\text{LPt}}$ , with the cooling-water flow rate,  $Q$ , the water-jet velocity,  $v_j$ , and the water-jet-impingement angle with respect to the vertical surface,  $\theta_j$ . The water-jet velocity,  $v_j$ , is a function of the water flow rate,  $Q$ , but also of the water-jet-hole cross section, *i.e.*, the DC mold design would appear to exert an influence on the occurrence of FB in the secondary cooling zone.

### III. METHODOLOGY

#### A. Water-Jet Rig

The secondary cooling in the DC casting of magnesium alloy AZ31 was investigated using a water-jet rig

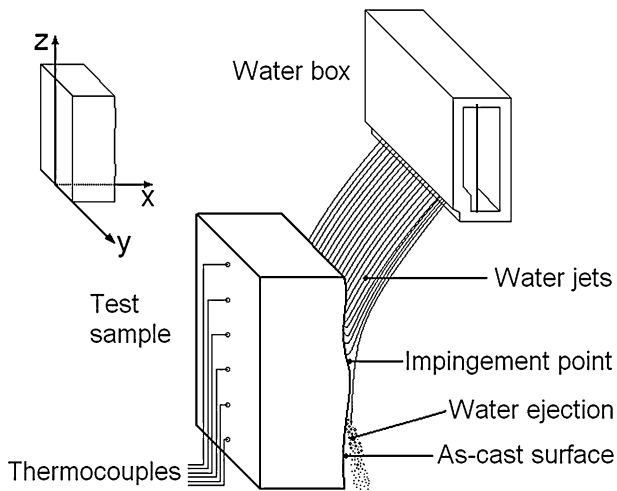


Fig. 4—Schematic of the water-jet experimental rig and definition of  $x$ ,  $y$ , and  $z$  directions.

shown on Figure 4. An electrical furnace heated up the instrumented sample to an initial temperature  $T_0$  between 300 °C and 500 °C prior to quenching. A water box with round, 4.75-mm-diameter holes produced jets of cooling water with a linear flow rate density (per unit width),  $Q'$ , between 85 and 150 L/min-m. Tubular inserts with an inner diameter of 3.18 mm allowed higher jet velocities and linear water flow rate densities between 50 and 125 L/min-m.

Samples with dimensions 250 × 150 × 100 mm were taken from an AZ31 bloom industrially cast at Timmenco Metals (Haley, ON, Canada). Figure 5 shows the typical “wavy” surface roughness of DC-cast AZ31. The vertical distance between two consecutive waves is approximately 20 mm, and the thickness of a wave is less than 1 mm. The sample face with the as-cast surface was the one exposed to the cooling water during a quenching experiment. The samples were instrumented with “E” type subsurface thermocouples inserted from the back of the sample. The disturbance of the temperature field caused by the 1.6-mm-diameter thermocouple holes was corrected using the “equivalent thermocouple depth” method developed at the University of British Columbia.<sup>[33,34]</sup>

The data acquisition rate during a cooling test was set to 50 Hz. The temperature signal presented a random noise amplitude of approximately 0.2 °C. Because of the very high sensitivity of the IHC analysis to noise, this signal was filtered using a five-point moving median followed by a five-point moving average. The possibility of a systematic temperature measurement bias was not considered, because the IHC analysis takes into account only the temperature variation.

Not shown on Figure 4 is the pneumatic displacement system, which could move the instrumented sample in order to simulate a “casting speed” between 10 and 40 mm/s. Quenching tests could also be conducted with a stationary sample by delaying the application of water jets until the sample had reached the bottom of its course. Both types of tests led to an ACF: an upward

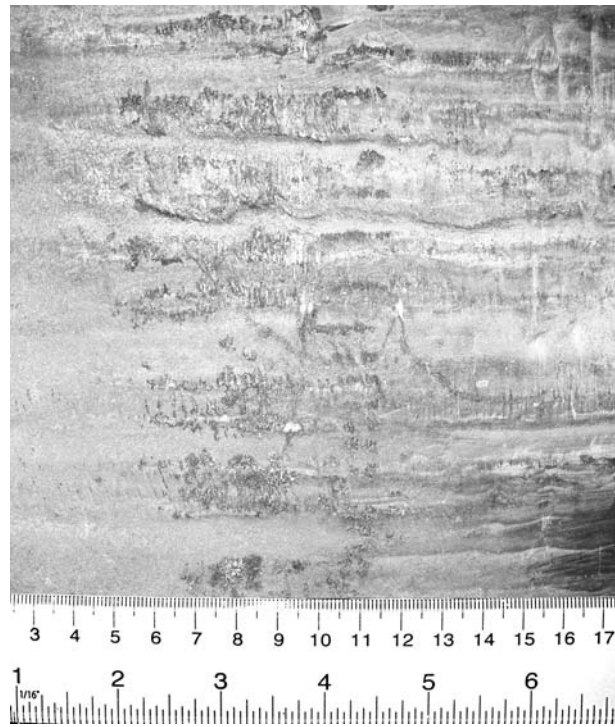


Fig. 5—Typical as-cast surface of AZ31 ingot.

ACF preceding the water-jet-impingement point in tests with a moving sample and a downward ACF preceding the free-falling water film in stationary experiments.

Despite the relatively small size of the instrumented samples, the limited initial temperature, and the sample moving speeds being approximately one order of magnitude higher than typical casting speeds, the experimental water-jet rig can be considered an accurate simulation of the full-scale DC casting process. As will be shown in Section IV, tests with a moving sample and stationary tests led to similar boiling curves (*e.g.*, in terms of CHF, slope in the TB regime, *etc.*). It can thus be safely concluded that tests conducted at an intermediate speed would also have produced the same results. Moreover, the sample thickness,  $x_{\max}$ , the thermophysical properties of AZ31, and the duration of a quench experiment,  $t_{\max}$ , were such that the corresponding Fourier number, calculated using Eq. [4], was below 0.10. This indicates that the instrumented sample could be considered a semi-infinite solid, and that larger samples would have led to the same results.

$$Fo = \frac{k_s t_{\max}}{\rho_s C_{p,s} (x_{\max})^2} \quad [4]$$

## B. IHC Analysis

The IHC algorithm used to convert the temperature history measured by the subsurface thermocouples into a boiling curve was based on Beck’s function specification method.<sup>[35]</sup> Figure 6 shows a schematic representation of this algorithm. As shown in Figure 6, the IHC

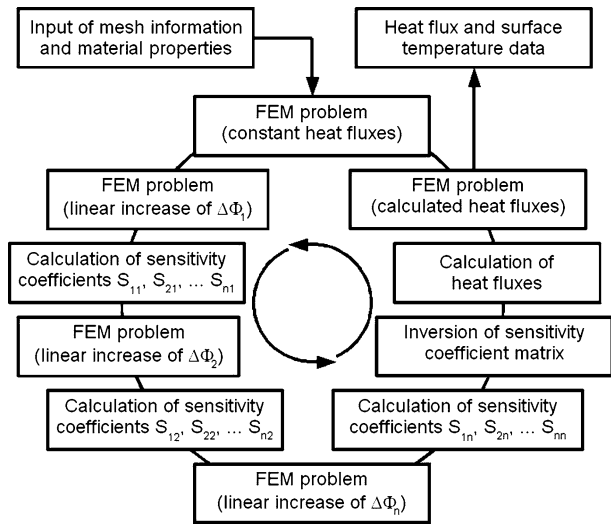


Fig. 6—Flowchart of IHC algorithm.

analysis solves a series of direct heat-conduction problems using the finite-element method (FEM) in order to build a system of  $n$  equations and  $n$  unknowns, in which  $n$  is the number of subsurface thermocouples. The  $n$  unknowns correspond to discrete heat-flux values that are used to model a continuous heat-flux profile along the  $z$  direction of the sample surface. The  $n$  equations are expressed as sensitivity coefficients, which represent the temperature change at a given thermocouple location for an arbitrary change in one of the discrete heat-flux values. Correspondingly, the relationship between the heat-flux change and the temperature variation measured by a subsurface thermocouple can be obtained by inverting the  $n \times n$  sensitivity coefficient matrix.

Three types of FEM problems were solved during an IHC analysis. An FEM problem conducted with constant heat-flux values and a series of FEM problems in which only one of the discrete heat-flux values was increased were used to evaluate the different sensitivity coefficients. In accordance with Beck's function specification method, these FEM problems were solved for a number,  $m$ , of future time-steps. The optimal number of future time-steps was found by trial and error: An IHC analysis was first conducted with two future time-steps, and this number was gradually increased until the calculated heat-flux values were stable, *i.e.*, did not diverge. Three to five future time-steps was the number of time-steps generally found to produce good results. The calculated heat-flux values were finally used as boundary conditions in an FEM simulation conducted for one single time-step, in order to provide the temperature profile for the next cycle.

The finite-element mesh that modeled the central section of the instrumented sample was a two-dimensional mesh made of 1651 rectangular elements. This two-dimensional model considered the central section of the sample, in which the thermocouples were located and heat was conducted in the  $x$  direction toward the quenched surface and in the  $z$  direction along the height of the sample. The heat flow in the  $y$  direction was

Table I. Thermophysical Properties of Magnesium AZ31 as Function of Temperature  $T$  (in  $^{\circ}\text{C}$ )<sup>[16]</sup>

| Thermophysical Property             | AZ31             |
|-------------------------------------|------------------|
| Thermal conductivity $k$ (W/m·K)    | $77.0 + 0.096 T$ |
| Specific heat $C_p$ (J/kg·K)        | $1000 + 0.666 T$ |
| Density $\rho$ (kg/m <sup>3</sup> ) | 1780.0           |

considered negligible, because the water flow was evenly distributed across the width of the sample during cooling experiments.

The partial differential equation governing two-dimensional transient heat conduction is given by Eq. [5]:

$$\frac{\partial}{\partial x} \left( k_x \frac{\partial T}{\partial x} \right) + \frac{\partial}{\partial z} \left( k_z \frac{\partial T}{\partial z} \right) = \rho C_p \frac{dT}{dt} \quad [5]$$

A heat-flux profile  $\Phi(z)$  formed with the  $n$  discrete heat fluxes was applied on one face of the mesh (Eq. [6]), whereas the other faces were adiabatic (Eqs. [7] through [9]):

$$-k \frac{\partial T}{\partial x} \Big|_{x=x_{\max}} = \Phi(z) \quad [6]$$

$$-k \frac{\partial T}{\partial z} \Big|_{z=0} = 0 \quad [7]$$

$$-k \frac{\partial T}{\partial z} \Big|_{z=z_{\max}} = 0 \quad [8]$$

$$-k \frac{\partial T}{\partial x} \Big|_{x=0} = 0 \quad [9]$$

Heat losses by natural convection and radiation on the sample sides were considered insignificant compared to the boiling-water heat transfer at the quenched surface. Typical heat fluxes for natural air convection are in the order of 10 kW/m<sup>2</sup>. The maximal heat loss by radiation (assuming an emissivity of 1.0) for a 600  $^{\circ}\text{C}$  surface is *circa* 30 kW/m<sup>2</sup>. The heat fluxes associated with boiling-water heat transfer, on the other hand, are generally in the order of MW/m<sup>2</sup>, *i.e.*, two orders of magnitude greater than the ones for natural air convection or radiation.

The initial temperature,  $T_0$ , at any given node was set as the first temperature measurement at the closest thermocouple location. The time-step length,  $\Delta t$ , used in the different FEM heat-conduction problems was equal to the thermocouple data acquisition period of 0.02 seconds. The thermophysical properties of magnesium AZ31 were a function of temperature and are presented in Table I.

The heat-flux profile,  $\Phi(z)$ , at the surface of the sample was modeled while taking into account the effect of the ACF. Previous research by Caron and Wells<sup>[36,37]</sup> highlighted the critical importance of taking into

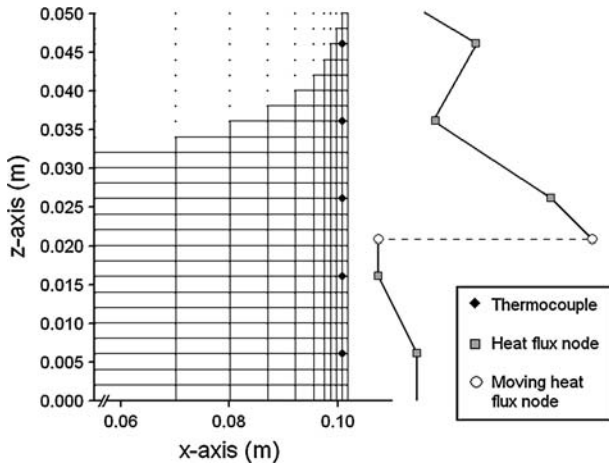


Fig. 7—Schematic of the heat-flux profile along the  $z$  direction and FEM mesh with thermocouple locations.

account the role of this phenomenon. As Figure 7 shows, the  $n$  discrete heat-flux profile values were assigned to nodes in front of the corresponding  $n$  thermocouples. Whereas these heat-flux nodes were stationary, an additional moving node was used to model the sharp drop in heat flux at the boundary between the wet and dry regions of the quenched surface. The value of the heat flux at this extra node was set as the maximum heat flux encountered previously in the stationary heat-flux node above it; it therefore did not change the number of unknowns in the linear system of  $n$  equations.

The position of the moving heat-flux node was determined prior to the IHC analysis by calculating the second derivative of the measured temperature with respect to time. This variable was evaluated using discrete temperature measurements according to Eq. [10]:

$$\frac{\partial^2 T}{\partial t^2} = \frac{T_{i+1} - 2T_i + T_{i-1}}{(\Delta t)^2} \quad [10]$$

The second derivative of the temperature with respect to time is known to reach a minimum when the heat-transfer mechanism is changed from natural air cooling to a boiling-water heat transfer.<sup>[38]</sup> The critical time at which this minimum was observed for a series of temperature measurements was thus set as the time at which the corresponding thermocouple is at the boundary between the wet and dry regions. The progression of this boundary between consecutive thermocouples was assumed to proceed at a constant speed. As Figure 8 shows, this assumption is valid for the case of a stationary sample.

## IV. RESULTS

### A. Low-Temperature Regimes

Semiempirical equations for the heat flux in the FC and NB regimes were developed by Weckman and Niessen<sup>[12]</sup> and were shown, in the compilation of

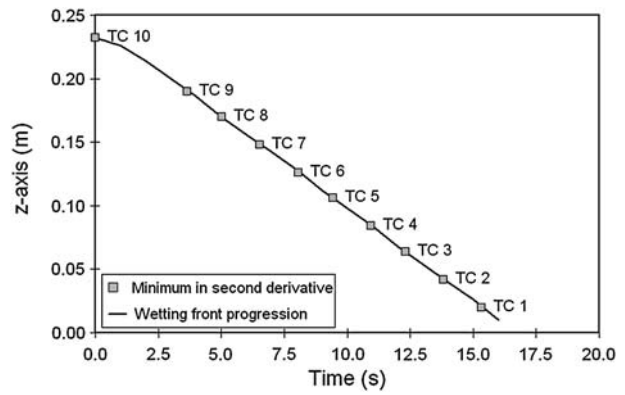


Fig. 8—Wetting front progression during FEM simulation of a cooling test.

boiling curves by Maenner *et al.*,<sup>[27]</sup> to be very accurate. According to Weckman and Niessen's research, the heat-transfer coefficient in the FC regime is a function of the cooling-water flow rate,  $Q$ , the billet diameter,  $D$ , the water temperature,  $T_f$ , and the surface temperature,  $T_s$ :

$$h_{FC,AL} = \left( 704 \left( \frac{T_s + T_f}{2} \right) + 2.53 \cdot 10^4 \right) \left( \frac{Q}{\pi D} \right)^{1/3} \quad [11]$$

in which the temperatures are expressed in degrees Celsius and the water flow rate  $Q$  is expressed in cubic meters per second. Equation [11] was developed for the secondary cooling of aluminum alloys in the water-film FFZ. The heat-transfer coefficient for the secondary cooling of magnesium AZ31 was similarly modeled by rearranging Eq. [11] and conducting a linear regression on experimental data:

$$\frac{h_{FC}}{(Q')^{1/3}} = \frac{\Phi_{FC}}{(T_s - T_f)(Q')^{1/3}} = C_1 T_s + C_2 T_f + C_3 \quad [12]$$

Equation [12] shows how the heat flux in the FC regime,  $\Phi_{FC}$ , divided by the temperature gradient,  $T_s - T_f$ , and the cubic root of the water flow rate density,  $Q'$  (expressed in L/min·m), is a linear function of the surface and water temperatures. The heat fluxes by FC in the water-jet IZ and the water-film FFZ are given by Eqs. [13] and [14], respectively. The higher heat-flux values in the IZ can be attributed to the greater turbulence caused by the water jets.

$$\Phi_{FC,IZ} = (16.6T_s + 71.6T_f - 541) \sqrt[3]{Q'} (T_s - T_f) \quad [13]$$

$$\Phi_{FC,FFZ} = (13.2T_s + 39.5T_f + 88) \sqrt[3]{Q'} (T_s - T_f) \quad [14]$$

The heat flux in the NB regime,  $\Phi_{NB}$ , was modeled by Weckman and Niessen<sup>[12]</sup> as the sum of the heat fluxes for FC and nucleate pool boiling (NPB).

$$\Phi_{NB} = \Phi_{FC} + \Phi_{NPB} \quad [15]$$

The contribution of NPB to the heat-flux  $\Phi_{NPB}$  was found to be a function of many different parameters (water thermophysical properties, temperature gradient,

surface tension forces between the ingot or billet surface, the water, and the ambient air, *etc.*), as described in Rohsenow's semiempirical equation:

$$\frac{C_{p,f}(T_s - T_{\text{sat}})}{i_{fg}} = C_f \left[ \Phi_{\text{NPB}} \left( \frac{1}{\mu_f i_{fg}} \right) \sqrt{\frac{\sigma_{fg}}{g(\rho_f - \rho_g)}} \right]^r \left( \frac{C_{p,f} \mu_f}{k_f} \right)^{1.7} \quad [16]$$

in which the parameters  $C_f$  and  $r$  are 0.016 and 0.33, respectively. Because the different properties of water are a function of the water temperature, Weckman and Niessen could considerably simplify Eq. [16] to:

$$\Phi_{\text{NPB,AL}} = 20.8(T_s - T_{\text{sat}})^3 \quad [17]$$

The effect of the specific thermophysical properties and surface roughness of magnesium AZ31 can be taken into account by modifying the coefficient and exponent in Eq. [17]. This was done by conducting a linear regression between the logarithms of the pool boiling contribution,  $\Phi_{\text{NB}} - \Phi_{\text{FC}}$ , and the temperature gradient,  $T_s - T_f$ . As can be seen in Eqs. [18] and [19], the NB regime for AZ31 is governed by a relatively low exponent compared to the one recommended by Weckman and Niessen for the secondary cooling of aluminum alloys:

$$\Phi_{\text{NPB,IZ}} = 4120(T_s - T_{\text{sat}})^{1.40} \quad [18]$$

$$\Phi_{\text{NPB,FFZ}} = 1.96(T_s - T_{\text{sat}})^{1.35} \quad [19]$$

Both parameters  $C_f$  and  $r$  in Eq. [16] have been known to depend on the thermophysical properties of the ingot material as well as the surface roughness. In particular, macroscopic surface roughness features such as scratches and scores generally increase the exponent  $r$  and thus decrease the slope of the boiling curve in the low-temperature NB regime.<sup>[39]</sup>

## B. Critical Heat Flux

Previous research with instrumented samples showed that the initial temperature plays a significant role in the measured surface heat flux.<sup>[27,31,40]</sup> Beyond a certain point, however, the initial sample temperature does not influence the boiling curve. The effect of other parameters (*e.g.*, water flow rate and water temperature) on the CHF,  $\Phi_{\text{CHF}}$ , could thus be identified by considering only the cooling tests conducted with a high initial temperature. As Figure 9 shows, the influence of the water flow rate on the CHF in the IZ can be quantified with a second-order equation:

$$\Phi_{\text{CHF,IZ}} = 8.8 \cdot 10^4 Q' - 2.5 \cdot 10^2 (Q')^2 \quad [20]$$

Whereas Yu<sup>[32]</sup> identified an effect of the water-jet velocity (for a constant water flow rate) on the CHF, such an effect was not observed in this research. The

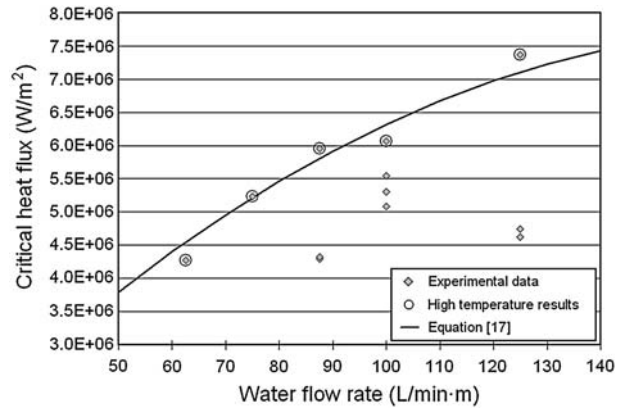


Fig. 9—Effect of cooling-water flow rate,  $Q'$ , on CHF,  $\Phi_{\text{CHF,IZ}}$ .

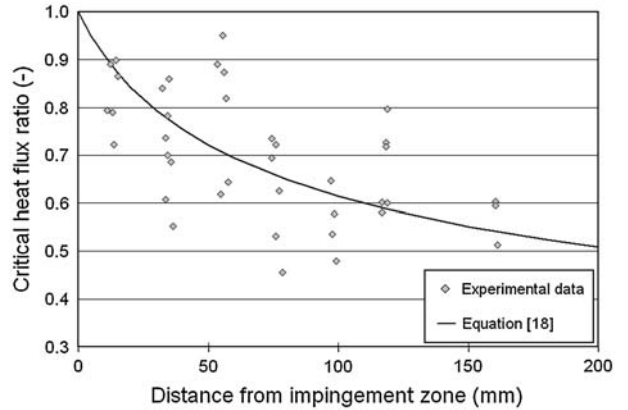


Fig. 10—Critical heat flux as function of distance from the IZ,  $d_{\text{IZ}}$ .

results presented in Figure 9 thus include both the low-velocity as well as the high-velocity cooling experiments.

The CHF in the water-film FFZ,  $\Phi_{\text{CHF,FFZ}}$ , was found to be a function of both the cooling-water flow rate,  $Q'$ , and the distance below the IZ,  $d_{\text{IZ}}$ . The effect of the distance below the IZ can be attributed to the increase in the cooling-water temperature that takes place as the water film flows down the surface. The CHF in the FFZ can be related to the corresponding CHF in the IZ by using the following equation:

$$\Phi_{\text{CHF,FFZ}} = \Phi_{\text{CHF,IZ}} (d_{\text{IZ}}/d_{79.4} + 1)^{-1/3} \quad [21]$$

in which the distance below the IZ,  $d_{\text{IZ}}$ , is expressed in mm and the parameter  $d_{79.4}$  is equal to 29.6 mm. According to Eq. [21], the CHF is equal to  $\Phi_{\text{CHF,IZ}}$  at a distance,  $d_{\text{IZ}}$ , of zero, and to 79.4 pct of  $\Phi_{\text{CHF,IZ}}$  at a distance of 29.6 mm. As Figure 10 shows, the relationship between the relative CHF,  $\Phi_{\text{CHF,IZ}}/\Phi_{\text{CHF,FFZ}}$ , and the distance from the IZ presents a significant amount of scatter. Bamberger and Prinz,<sup>[41]</sup> in their study of the water blade jet cooling of various metals, also found similar levels of data scatter. This can be attributed to the multiplication of measurement errors in  $d_{\text{IZ}}$ ,  $\Phi_{\text{CHF,IZ}}$ , and  $\Phi_{\text{CHF,FFZ}}$ .

### C. Transition Boiling

Cooling experiments conducted with both stationary and moving samples showed a strong influence of the initial sample temperature,  $T_0$ , and the sample moving speed,  $v_c$ , on the heat flux in the TB regime. However, these two effects can be reduced to a single parameter, namely, the initial temperature at the impingement point,  $T_{0,IZ}$ . Because of the ACF phenomenon that takes place at the sample surface, a slow-moving sample will have time to cool down before the impingement with the water jets, and the boiling curve will correspondingly start at a lower temperature. Cooling tests conducted with a stationary sample, however, will produce a boiling curve that starts at the initial sample temperature,  $T_0$ .

As seen on Figure 11, the effect of the initial temperature at the water-jet-impingement point is actually limited to the temperature at which the boiling curve begins. The slope of the boiling curve as the TB regime begins was found to be independent of the cooling-water flow rate, initial casting speed, and sample moving speed. In boiling curves for the secondary cooling of magnesium AZ31, this slope is equal to  $-4.5 \cdot 10^4 \text{ W/m}^2 \text{ }^\circ\text{C}$  in the water-jet IZ and  $-5.0 \cdot 10^4 \text{ W/m}^2 \text{ }^\circ\text{C}$  in the water-film FFZ. Moreover, the heat-transfer coefficient in the TB regime,  $h_{TB}$ , was found to increase linearly as the boiling-water heat transfer progresses from the TB to the CHF. Knowledge of the initial slope can thus be used to model this heat-transfer coefficient for the entire TB regime:

$$h_{TB,IZ} = h_{NAC} - \left( \frac{d\Phi}{dT} \right)_{TB} \frac{(T_{0,IZ} - T_s)}{(T_{0,IZ} - T_f)} \quad [22]$$

$$h_{TB,FFZ} = h_{NAC} - \left( \frac{d\Phi}{dT} \right)_{TB} \frac{(T_{wet} - T_s)}{(T_{wet} - T_f)} \quad [23]$$

in which  $h_{NAC}$  is the heat-transfer coefficient for natural air convection, whereas  $T_{0,IZ}$  is the initial temperature at the water-jet-impingement point and  $T_{wet}$  is the water-film rewetting temperature.

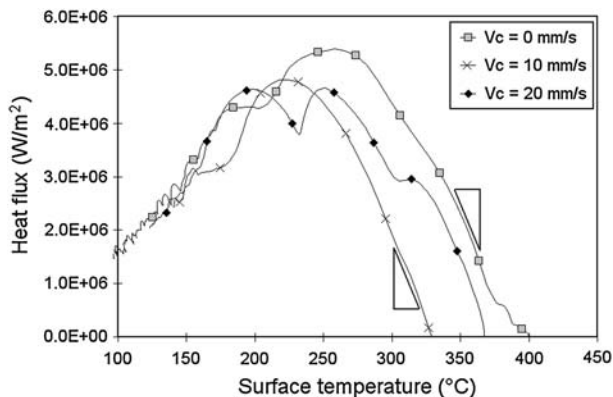


Fig. 11—Calculated boiling curves for different sample moving speeds,  $v_c$ <sup>[42]</sup> (AA5182,  $T_0 = 400 \text{ }^\circ\text{C}$ ,  $Q' = 100 \text{ L/min}\cdot\text{m}$ ).

### D. Film Boiling

Stable FB was not observed in the water-jet IZ during quenching tests with instrumented AZ31 samples. This was probably due to the relatively low thermal effusivity,  $\epsilon_{th}$ , of magnesium. The thermal effusivity of a material is given by Eq. [24] and is a measure of the material's ability to provide heat to its environment:

$$\epsilon_{th} = \sqrt{k_s \rho_s C_{p,s}} \quad [24]$$

Materials with a high thermal effusivity can transfer heat very rapidly to a wet spot at the surface and thus prevent the breakdown of the vapor layer. Correspondingly, a material with a lower thermal effusivity such as magnesium AZ31 has a tendency to form stable wet spots and is thus associated with a high Leidenfrost point temperature,  $T_{LPt}$ .

Cooling tests conducted on aluminum AA5182 samples provided a relationship between the Leidenfrost point temperature and the cooling-water flow rate.<sup>[42]</sup> This relationship is given by Eq. [25]:

$$T_{LPt,AA5182} = 100.0 + 33.0\sqrt{Q'} \quad [25]$$

The Leidenfrost point for the secondary cooling of other materials can be calculated by taking into account the difference in thermal effusivity, as shown in Eq. [26]:

$$T_{LPt} = 100.0 + [33.0 + 0.00085(\epsilon_{th,AA5182} - \epsilon_{th})]\sqrt{Q'} \quad [26]$$

This equation was developed from research conducted by Jeschar *et al.*<sup>[43]</sup> on the vapor layer breakdown temperature at the surface of different materials, which showed a linear relationship between the Leidenfrost point temperature,  $T_{LPt}$ , and the thermal effusivity,  $\epsilon_{th}$ .

As Figure 12 shows, all cooling tests conducted with low-velocity water jets started at a temperature below the corresponding model Leidenfrost point,  $T_{LPt}$ , for AZ31. Safety concerns prevented the use of higher initial temperatures. High-velocity water jets are associated with even higher Leidenfrost point temperatures, as

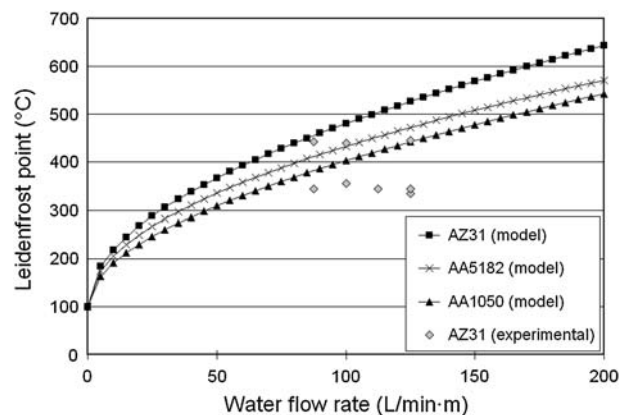


Fig. 12—Modeled and measured Leidenfrost point,  $T_{LPt}$ , as function of water flow rate,  $Q'$ .



reported by Yu;<sup>[32]</sup> stable FB is therefore even more difficult to observe in such conditions.

Stable FB occurs in the water-jet-impingement point, because the horizontal component of the water-jet momentum compensates for the pressure associated with the formation of steam, thus trapping the cooling water between the vapor layer and the water jets. In the water-film FFZ, however, there is no horizontal force to oppose the formation of steam, and the cooling-water film is ejected from the surface at high temperatures. The minimum temperature at which water-film ejection takes place is referred to as the wetting temperature,  $T_{\text{wet}}$ . Above this temperature, the ingot or billet surface is dry and cooling occurs by natural air convection. Below this temperature, the surface is at least partially wet and TB takes place.

The wetting temperature,  $T_{\text{wet}}$ , was found to be strongly correlated with the initial sample temperature,  $T_0$ . This observation underlines the transient nature of the water-film ejection, because the criterion as to whether the water film will be ejected depends on the temperature history at this point of the surface. This would indicate that the free-falling water film requires a certain “incubation” time to wet the surface, and that this incubation time increases with the initial temperature. Moreover, the wetting temperature was also found to increase with the cooling-water flow rate. Obviously, a higher flow rate is associated with a thicker water film, which is more difficult to eject from the surface.

The combined effect of the initial temperature,  $T_0$ , and the cooling-water flow rate,  $Q'$ , was evaluated by assuming that the wetting temperature,  $T_{\text{wet}}$ , was governed by an equation similar to Eqs. [25] and [26] for the Leidenfrost temperature. This assumption was based on the idea that the water-film ejection and stable FB are related phenomena. As Eq. [27] shows, the influence of the cooling-water flow rate,  $Q'$ , is minimal compared to its effect on the Leidenfrost temperature.

$$T_{\text{wet}} = 100.0 + (0.00126T_0^2 - 0.666T_0 + 210.6)(Q')^{0.115} \quad [27]$$

Figure 13 compares the measured wetting temperatures with the corresponding modeled wetting temperatures calculated with Eq. [27]. The model was found to be

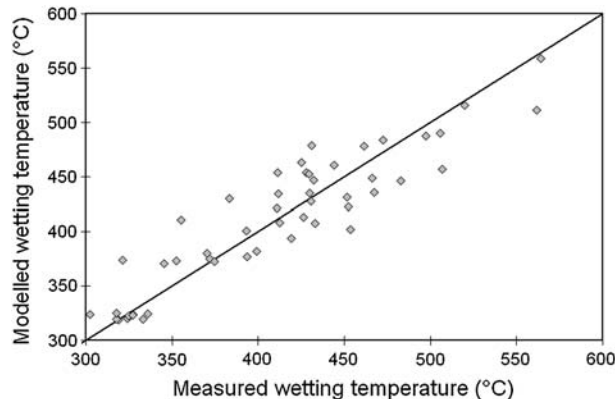


Fig. 13—Modeled and calculated wetting temperatures,  $T_{\text{wet}}$ .

very accurate ( $R^2 = 0.885$ ) for the range of experimental conditions investigated in this research: an initial temperature,  $T_0$ , between 300 °C and 550 °C and a cooling-water flow rate,  $Q'$ , between 50 and 125 L/min-m.

## V. DISCUSSION

The different results presented in Section IV can be combined to build idealized boiling curves in which the intersection points between curve segments correspond to the transition temperatures between boiling regimes. Figure 14 illustrates such an idealized boiling curve for the water-jet IZ. It also shows a boiling curve calculated according to Hao’s model,<sup>[2]</sup> with the same parameters: a cooling-water flow rate,  $Q'$ , of 50 L/min-m, a water temperature,  $T_f$ , of 37.8 °C, and an initial temperature,  $T_{0,IZ}$ , of 510 °C. As Figure 14 shows, both curves present a very good agreement in the FC and NB regimes. However, the boiling curve based on the DC casting of aluminum alloys is characterized by a significantly lower Leidenfrost point temperature, as well as by lower heat fluxes in the TB regime and at the CHF. The lower Leidenfrost point of aluminum alloys was already discussed in Figure 11.

Figure 15 compares boiling curves for the IZ and a relatively high cooling-water flow rate of 125 L/min-m. In comparison with the idealized boiling curve calculated with the equations presented in Section IV, the boiling curve evaluated according to Hao’s model presents a greater heat flux in the FC and NB regime. This discrepancy would indicate that the effect of the cooling-water flow rate on low-temperature boiling regimes is not purely linear. Moreover, the boiling curves depicted in Figure 15 differ considerably in the TB and FB regimes. This result underlines the importance of taking into account the effect of the cooling-water flow rate and material thermophysical properties on the Leidenfrost point.

Figure 16 shows the boiling curves for the water-film FFZ and a low cooling-water flow rate,  $Q'$ , of 50 L/min-m. The idealized boiling curve was calculated with a distance from the IZ,  $d_{IZ}$ , of zero. The most significant

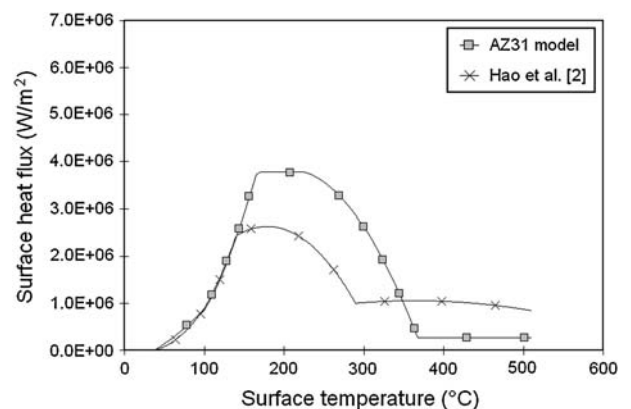


Fig. 14—Boiling curve comparison for the water-jet IZ ( $Q' = 50$  L/min-m,  $T_0 = 510$  °C,  $T_f = 37.8$  °C).

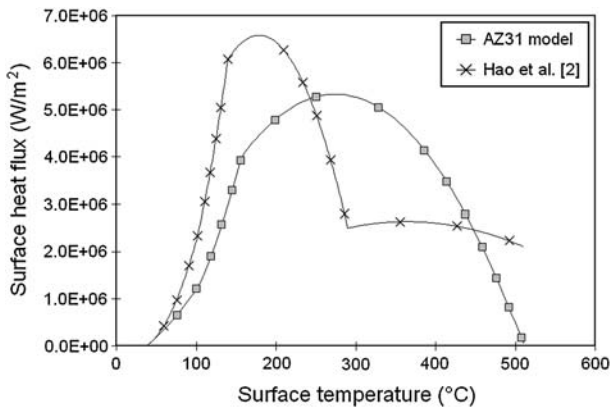


Fig. 15—Boiling curve comparison for the water-jet IZ ( $Q' = 125 \text{ L/min-m}$ ,  $T_0 = 510 \text{ }^\circ\text{C}$ ,  $T_f = 37.8 \text{ }^\circ\text{C}$ ).

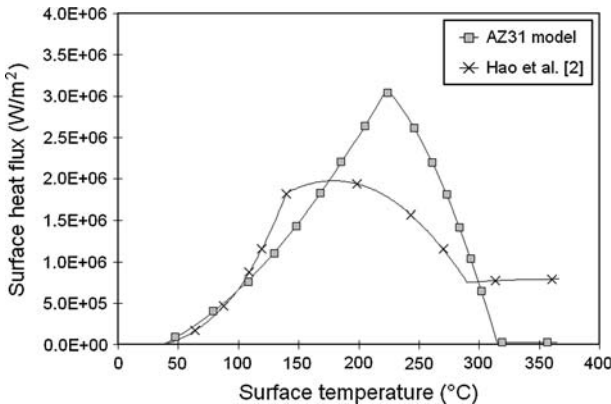


Fig. 16—Boiling curve comparison for the water-film FFZ ( $Q' = 50 \text{ L/min-m}$ ,  $T_0 = 510 \text{ }^\circ\text{C}$ ,  $T_f = 37.8 \text{ }^\circ\text{C}$ ).

difference between the two boiling curves is the absence of stable FB in the idealized boiling curve. The very low heat flux that takes place above the wetting temperature corresponds to natural air convection. In comparison, the boiling curve calculated according to Hao's model overestimates the heat flux at high surface temperatures.

Idealized boiling curves can also be compared to results published by Hibbins<sup>[16]</sup> for the DC casting of magnesium alloys. In the water-film FFZ, the reported heat-transfer coefficients of 10,000 to 12,000  $\text{W/m}^2\text{-K}$  are only in agreement with the low-temperature regimes of the idealized boiling curve, *i.e.*, FC and NB. In the water-jet IZ and the relatively low heat-transfer coefficients identified by Hibbins correspond to an average value for the TB and FB regimes, but cannot accurately represent the heat-flux increase between the Leidenfrost point and the CHF. Moreover, these heat-transfer coefficients are significantly lower than the idealized boiling curve in the NB and FC regimes.

## VI. SUMMARY AND CONCLUSIONS

The DC casting of magnesium is associated with defects such as surface folds and center cracks.

Mathematical models can provide a better understanding of the DC casting process and help prevent the formation of defects but require accurate boundary conditions for the primary cooling and secondary cooling zones. A review of the published literature showed the absence of reliable data for the secondary cooling of magnesium alloys in the DC casting process. However, research previously conducted on the secondary cooling of aluminum alloys provided insight into the effect of various parameters on the different boiling regimes. In order to simulate the secondary cooling zone, magnesium AZ31 samples were instrumented with subsurface thermocouples and quenched with jets of cooling water. An IHC analysis was conducted on the temperature history measured by the thermocouples and provided information on the different boiling-water heat-transfer phenomena that take place during quenching. The relationship between the heat flux and surface temperature during a cooling experiment was expressed as a boiling curve. The effect of the cooling-water flow rate, water temperature, water-jet velocity, and initial sample temperature on segments of the boiling curve was investigated. The different equations developed in this research could be combined to form idealized boiling curves. A comparison between these idealized boiling curves and the boiling curves originally developed for the DC casting of aluminum alloys highlighted significant differences between the secondary cooling of the two light metals.

## NOMENCLATURE

### LATIN SYMBOLS

|           |  |
|-----------|--|
| $C_f$     | coefficient in Rohsenow's NPB model (—)  |
| $C_p$     | specific heat ( $\text{J kg}^{-1} \text{K}^{-1}$ )   |
| $D$       | billet diameter (m)  |
| $d_{IZ}$  | distance from water-jet IZ (mm)  |
| $Fo$      | Fourier number (—)   |
| $g$       | gravitational acceleration ( $\text{m s}^{-2}$ )   |
| $h$       | heat-transfer coefficient ( $\text{W m}^{-2} \text{K}^{-1}$ )                                  |
| $i_{fg}$  | latent heat of evaporation ( $\text{J kg}^{-1}$ )  |
| $k$       | thermal conductivity ( $\text{W m}^{-1} \text{K}^{-1}$ )                                       |
| $Q$       | volumetric cooling-water flow rate ( $\text{m}^3 \text{s}^{-1}$ )                              |
| $Q'$      | volumetric cooling-water flow rate per unit of perimeter ( $\text{L min}^{-1} \text{m}^{-1}$ ) |
| $r$       | exponent in Rohsenow's NPB model (—)   |
| $T_0$     | initial temperature ( $^\circ\text{C}$ )   |
| $T_f$     | water bulk temperature ( $^\circ\text{C}$ )  |
| $T_{LPt}$ | Leidenfrost point temperature ( $^\circ\text{C}$ )   |
| $T_{ONB}$ | onset of NB temperature ( $^\circ\text{C}$ )   |
| $T_s$     | surface temperature ( $^\circ\text{C}$ )   |
| $T_{sat}$ | water saturation temperature ( $^\circ\text{C}$ )  |
| $T_{wet}$ | rewetting temperature ( $^\circ\text{C}$ )   |
| $t$       | time (s)   |
| $v_c$     | sample moving speed ( $\text{mm s}^{-1}$ )   |
| $v_f$     | water-jet velocity ( $\text{m s}^{-1}$ )   |
| $x$       | sample thickness dimension (m)   |
| $z$       | sample height dimension (m)  |

## GREEK SYMBOLS

|                    |  |
|--------------------|--|
| $\Delta t$         | time-step length (s)   |
| $\varepsilon_{th}$ | thermal effusivity ( $\text{J m}^{-2} \text{K}^{-1} \text{s}^{-0.5}$ ) |
| $\Phi$             | heat flux ( $\text{W m}^{-2}$ )  |
| $\mu_f$            | water viscosity ( $\text{kg m}^{-1} \text{s}^{-1}$ )                   |
| $\theta_f$         | water-jet-impingement angle (deg)                                      |
| $\rho$             | density ( $\text{kg m}^{-3}$ )   |
| $\sigma_{fg}$      | surface tension at the water/steam interface ( $\text{N m}^{-1}$ )     |

## REFERENCES

- P. Baker: *Light Met. (Métaux Légers)*, 1997, pp. 355–67.
- H. Hao, D.M. Maijer, M.A. Wells, S.L. Cockcroft, D. Sediako, and S. Hibbins: *Metall. Mater. Trans. A*, 2004, vol. 35A, pp. 3842–54.
- J.F. Grandfield, A. Hoadley, and S. Instone: *Light Met.*, 1997, pp. 691–99.
- J. Sengupta, S.L. Cockcroft, D.M. Maijer, M.A. Wells, and A. Larouche: *Metall. Mater. Trans. B*, 2004, vol. 35B, pp. 532–39.
- J. Sengupta, S.L. Cockcroft, D.M. Maijer, M.A. Wells, and A. Larouche: *J. Light Met.*, 2002, vol. 2, pp. 137–48.
- W. Roth: *Aluminium*, 1943, pp. 283–91.
- H. Klein: *Giesserei*, 1953, vol. 10, pp. 441–54.
- R. Siegel: *Int. J. Heat Mass Transfer*, 1978, vol. 21, pp. 1421–30.
- D.J.P. Adenis, K.H. Coats, and D.V. Ragone: *J. Inst. Met.*, 1962–1963, vol. 91, pp. 395–403.
- D.A. Peel and A.E. Pengelly: *Mathematical Models in Metallurgical Process Development*, Iron and Steel Institute, 1969, pp. 186–96.
- D.C. Weckman, R.J. Pick, and P. Niessen: *Z. Metallkd.*, 1979, vol. 70 (11), pp. 750–57.
- D.C. Weckman and P. Niessen: *Metall. Trans. B*, 1982, vol. 13B, pp. 593–602.
- J. Du, B.S.J. Kang, K.M. Chang, and J. Harris: *Light Met.*, 1998, pp. 1025–30.
- G.P. Greal, J.L. Davis, E.K. Jensen, P.A. Tøndel, and J. Moritz: *Light Met.*, 2001, pp. 813–21.
- J.G. Collier and J.R. Thome: *Convective Boiling and Condensation*, 4th ed., Oxford University Press, Oxford, United Kingdom, 1996, pp. 148–69.
- S.G. Hibbins: *Light Met. (Métaux Légers)*, 1998, pp. 265–80.
- Q.C. Le, S.J. Guo, Z.H. Zhao, J.Z. Cui, and X.J. Zhang: *J. Mater. Process. Technol.*, 2007, vol. 183, pp. 194–201.
- H. Yu: *Light Met.*, 1985, pp. 1331–47.
- J. Langlais, T. Bourgeois, Y. Caron, G. Béland, and D. Bernard: *Light Met.*, 1995, pp. 979–86.
- E.K. Jensen, S. Johansen, T. Bergström, and J.A. Bakken: *Light Met.*, 1986, pp. 891–96.
- J.A. Bakken and T. Bergström: *Light Met.*, 1986, pp. 883–89.
- E.D. Tarapore: *Light Met.*, 1989, pp. 875–80.
- J.B. Wiskel and S.L. Cockcroft: *Metall. Mater. Trans. B*, 1996, vol. 27B, pp. 119–27.
- J.B. Wiskel and S.L. Cockcroft: *Metall. Mater. Trans. B*, 1996, vol. 27B, pp. 129–37.
- K. Kuwana, S. Viswanathan, J.A. Clark, A. Sabau, M.I. Hassan, K. Saito, and S. Das: *Light Met.*, 2005, pp. 989–93.
- H. Kraushaar, R. Jeschar, V. Heidt, E.K. Jensen, and W. Schneider: *Light Met.*, 1995, pp. 1055–59.
- L. Maenner, B. Magnin, and Y. Caratini: *Light Met.*, 1997, pp. 701–07.
- A. Larouche, Y. Caron, and D. Kocafe: *Light Met.*, 1998, pp. 1059–64.
- I.J. Opstelten and J.M. Rabenberg: *Light Met.*, 1999, pp. 729–35.
- L.I. Kiss, T. Meenken, A. Charette, Y. Lefebvre, and R. Lévesque: *Light Met.*, 2002, pp. 981–85.
- M.A. Wells, D. Li, and S.L. Cockcroft: *Metall. Mater. Trans. B*, 2001, vol. 32B, pp. 929–39.
- H. Yu: *Light Met.*, 2005, pp. 983–87.
- E. Caron, M.A. Wells, and D. Li: *Metall. Mater. Trans. B*, 2006, vol. 37B, pp. 475–83.
- G.A. Franco, E. Caron, and M.A. Wells: *Metall. Mater. Trans. B*, 2007, vol. 38B, pp. 949–56.
- J.V. Beck, B. Blackwell, and C.R. St. Clair, Jr.: *Inverse Heat Conduction: Ill-Posed Problems*, John Wiley & Sons, Hoboken, NJ, 1985, pp. 108–61.
- E. Caron and M.A. Wells: *Proc. 10th Int. Conf. Aluminum Alloys*, Vancouver, BC, Canada, 2006.
- E. Caron and M.A. Wells: *Aluminium Cast House Technol. 2007—Proc. 10th Australasian Conf. Exhib.*, Sydney, NSW, Australia, 2007.
- J. Filipovic, F.P. Incropera, and R. Viskanta: *Exp. Heat Transfer*, 1995, vol. 8, pp. 257–70.
- R.I. Vachon, G.E. Tanger, D.L. Davis, and G.H. Nix: *J. Heat Transfer*, 1968, pp. 239–47.
- D. Li, M.A. Wells, S.L. Cockcroft, and E. Caron: *Metall. Mater. Trans. B*, 2007, vol. 38B, pp. 901–10.
- M. Bamberger and B. Prinz: *Mater. Sci. Technol.*, 1986, vol. 2, pp. 410–15.
- E. Caron and M.A. Wells: *Aluminium Alloys: Their Physical and Mechanical Properties—Proc. 11th Int. Conf. Aluminum Alloys*, Aachen, Germany, 2008.
- R. Jeschar, U. Reiners, and R. Scholz: *Steelmaking Proc.*, 1986, vol. 69, pp. 511–21.